


Palladium/graphene oxide nanocomposites with carbon nanotubes and/or magnetite for the reduction of nitrophenolic compounds

L.K. Parrott, E. Erasmus* 

Supplementary Information

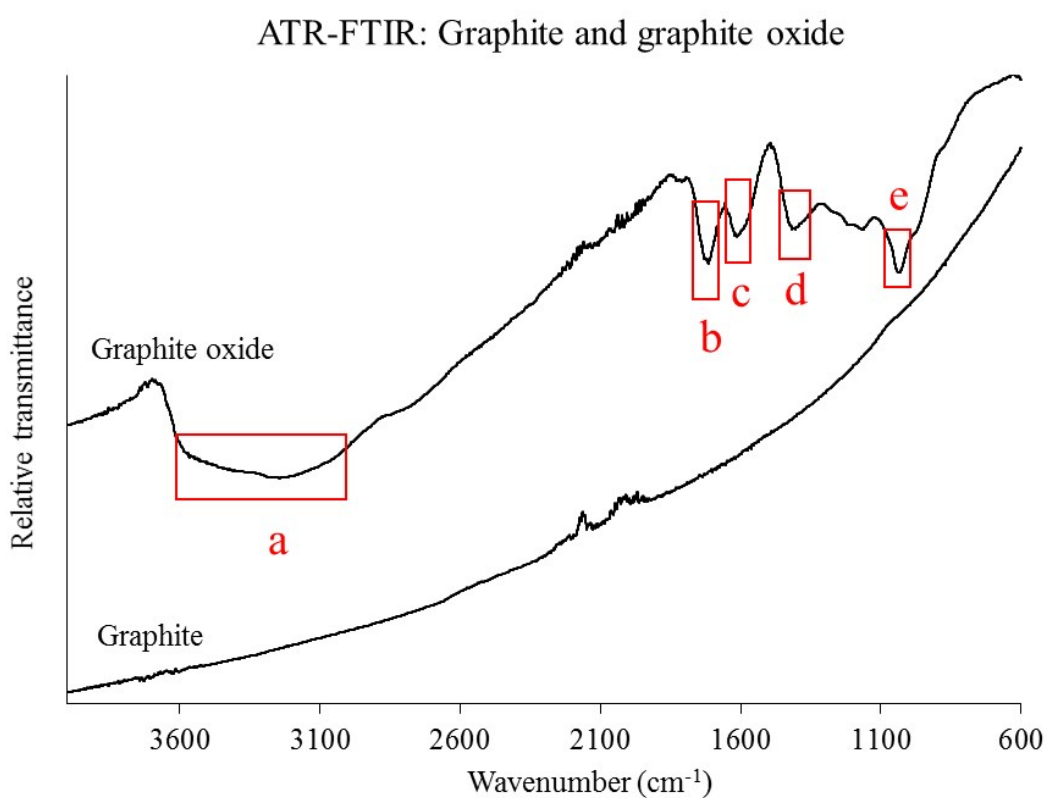


Figure S1. FTIR-ATR spectra of graphite (below) and graphite oxide (above). (a), represents the O-H stretching frequencies, including of water. (c) is also an indicator of -OH functionalities. (b-e) is assigned to C=O, C-OH and C-O stretching frequencies respectively.

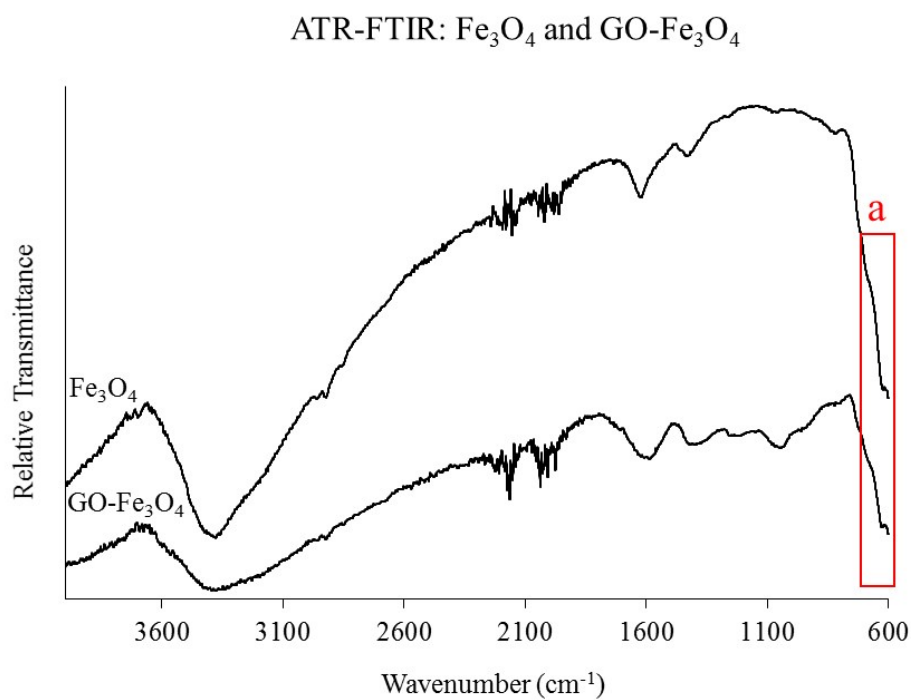


Figure S2. FTIR-ATR showing Fe₃O₄ and its composite with GO, GO-Fe₃O₄. (a) the shoulder forms part of the characteristic band of iron oxide nanoparticles around 570-580 cm⁻¹.

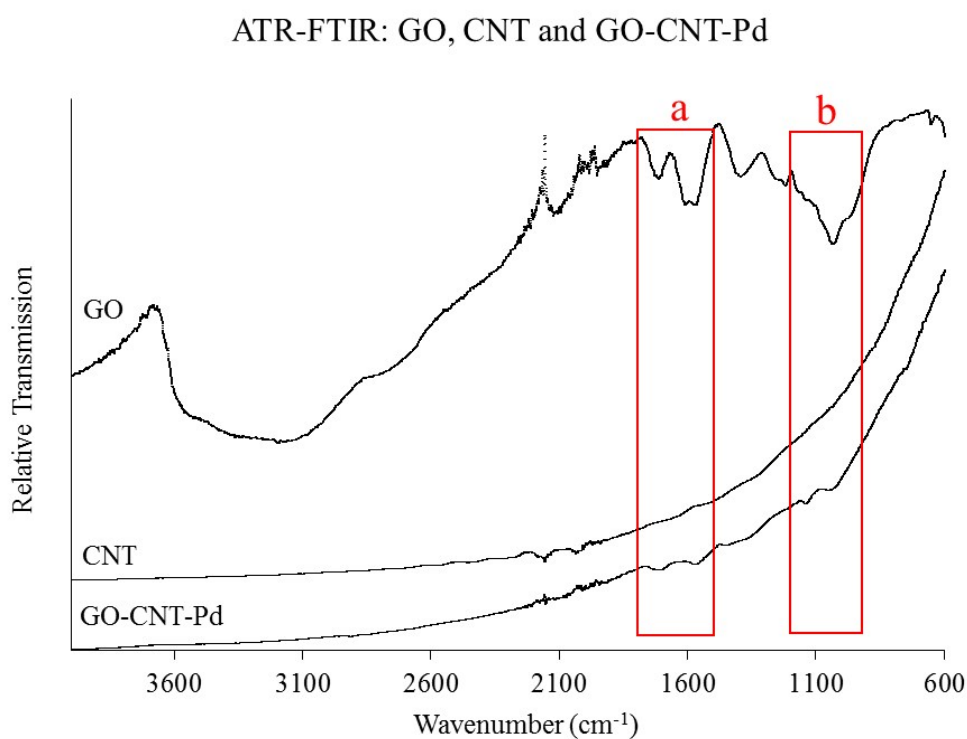


Figure S3. FTIR-ATR showing GO, CNT and GO-CNT-Pd

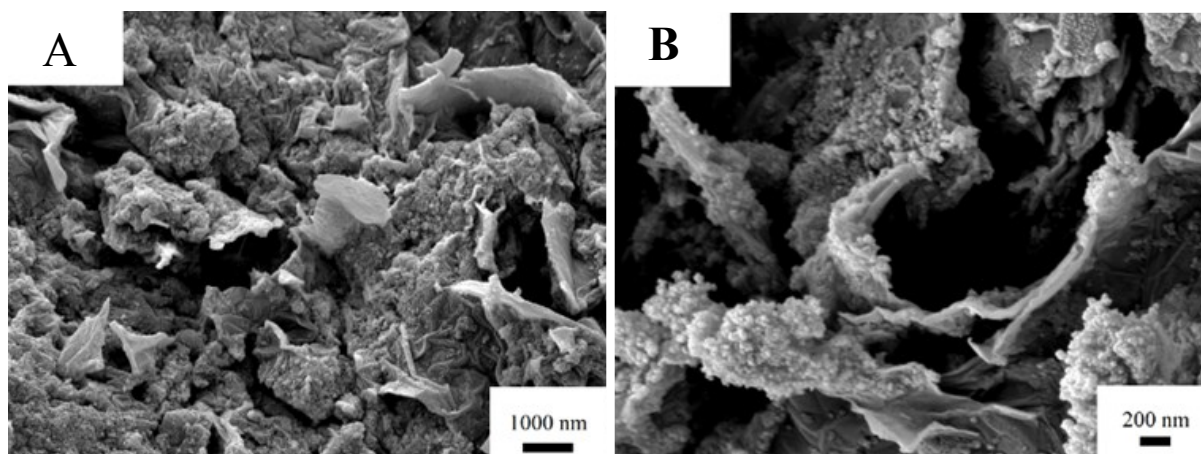


Figure S4. SEM of Fe₃O₄/GO at (A) scale 1000 nm and (B) scale 200 nm.

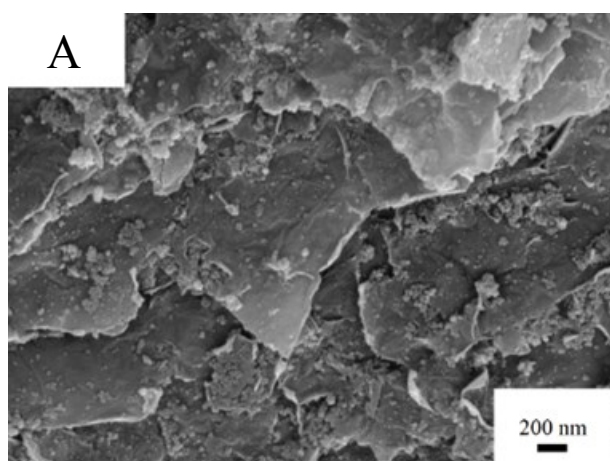


Figure S5. SEM of (A) Pd/Fe₃O₄/GO.

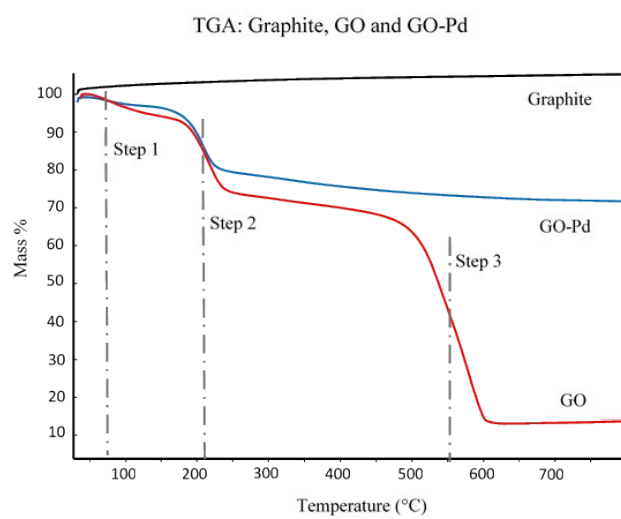


Figure S6. The TGA of Graphite, graphite oxide and GO-Pd.

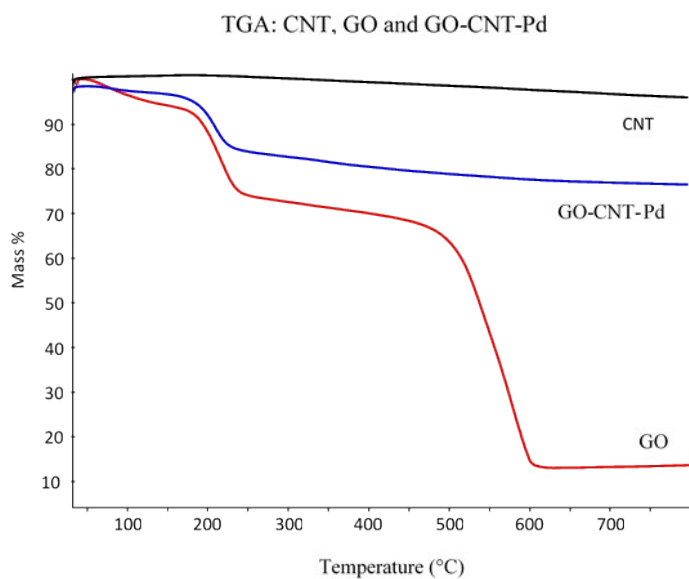


Figure S7. Thermogram of graphite oxide, CNT and GO-CNT-Pd.

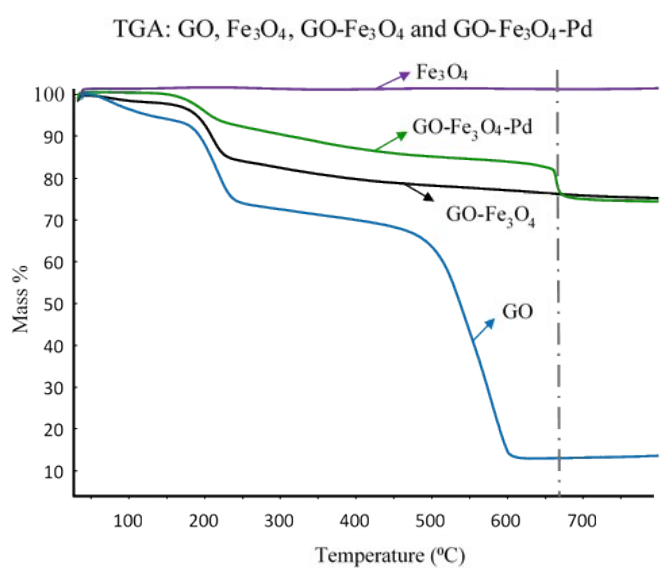


Figure S8. The thermograms of GO, Fe₃O₄, GO-Fe₃O₄ and GO-Fe₃O₄-Pd.

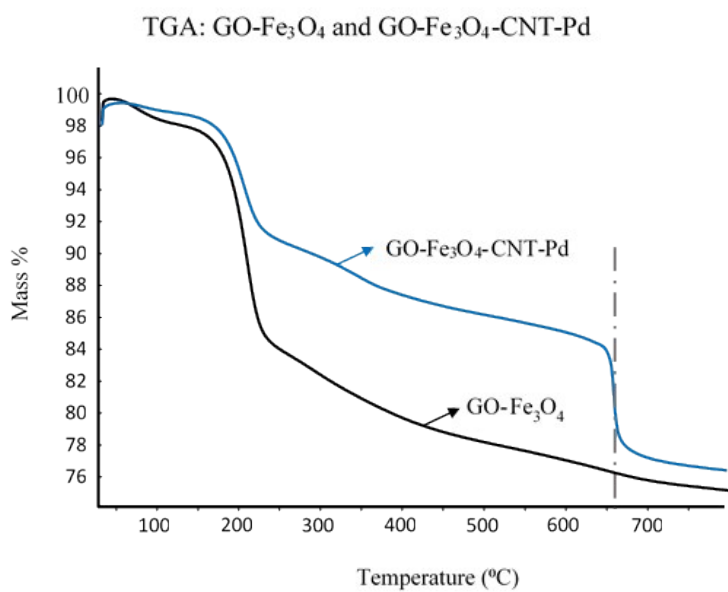


Figure S9. Thermogram showing GO-Fe₃O₄ (precursor) and GO-Fe₃O₄-CNT-Pd

Table S1. Binding energies (eV) of Pd 3d

Compound	Binding energies (eV)			
	Pd(0)		Pd(II)	
	3 d _{5/2}	3 d _{3/2}	3 d _{5/2}	3 d _{3/2}
GO-Pd	335.60	340.84	337.95	343.12
GO-Fe ₃ O ₄ -Pd	335.55	340.81	336.58	341.84
GO-Fe ₃ O ₄ -Pd (spent)	335.66	340.92	338.31	343.57
GO-CNT-Pd	335.61	340.87	337.78	343.04
GO-Fe ₃ O ₄ -CNT-Pd	335.55	340.81	337.45	342.71

Table S2. Binding energies (eV) of Fe 2p

Compound	Binding energies (eV) of Fe	
	2 p _{1/2}	2 p _{3/2}
Fe ₃ O ₄	723.28	709.89
GO-Fe ₃ O ₄	722.15	710.74
GO-Fe ₃ O ₄ -Chit	722.75	710.47
GO-Fe ₃ O ₄ -Pd	723.05	710.81
GO-Fe ₃ O ₄ -Pd (spent)	723.89	710.85
GO-Fe ₃ O ₄ -CNT-Pd	723.05	710.95

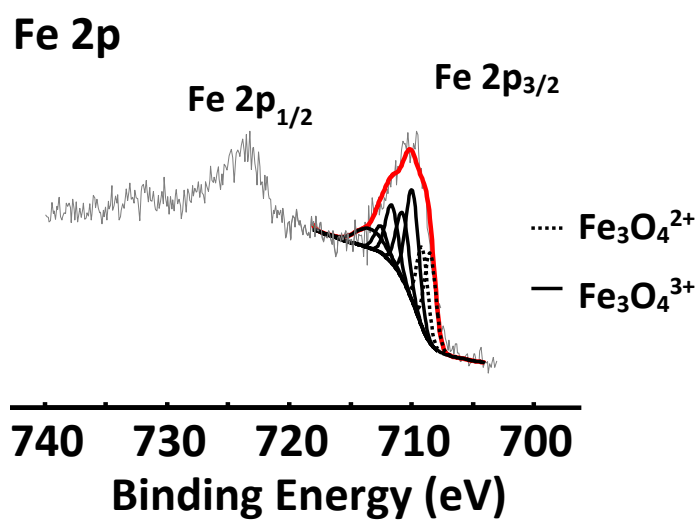


Figure S10. The XPS of the Fe 2p photoelectron line of Fe₃O₄ nanoparticles, showing the deconvolution of the Fe 2p_{3/2} into the Fe^{II} and Fe^{III} species according to the fitting parameters of Biesinger *et. al.*

Apparent optical band energy, α' .

UV-Vis characterisation of the four nanocomposites in suspension (ca. 1 mg in 5 ml water) was measured on an Olis Clarity CCD UV/Vis Spectroscopic system.

The broad absorption peaks observed for the four nanocomposites, in the short wavelength area are related to the intrinsic band gap energy of nanocomposite. The classical Tauc equation was employed to determine the apparent band gap energy, E_g' , of the nanocomposites (the term apparent is used since this is not a thin film but nanocrystals):

$$\alpha E_p = K(E_p - E_g)^{1/2}$$

where α is the absorption coefficient ($\alpha = \ln(T/d)$, where T = transmission and d = thickness, average thickness of the GO was used, ca. 3 nm), K is a constant, E_p is photon energy ($E_p = hc/\lambda$, h = Planck's constant and c = speed of light), and E_g is the band gap energy. The extrapolate value (E_p at $\alpha = 0$) of the straight line to the X-axis of the graph of $(\alpha E_p)^2$ versus E_p , represents the apparent band gap energy.

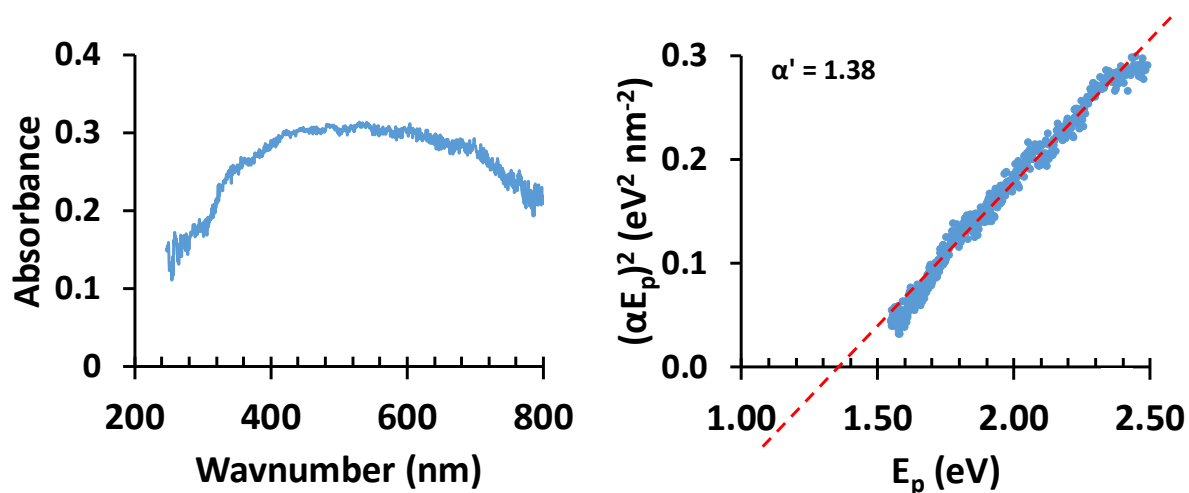


Figure S11. Left: The UV-Visible spectra of Pd-GO (0.8 mg/5 ml water). Right: The Tauc plot of Pd-GO used to determine the apparent band gap energy, E_g' .

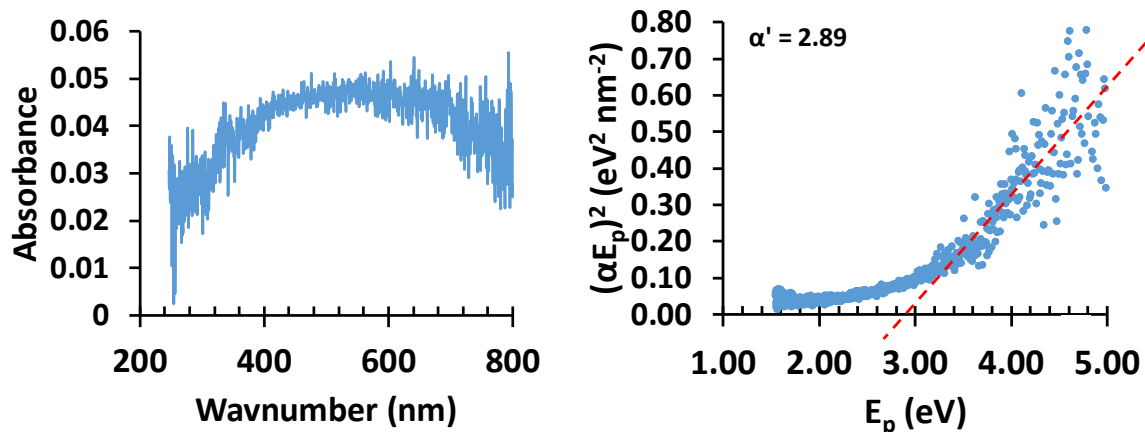


Figure S12. Left: The UV-Visible spectra of Pd-Fe₃O₄-GO (0.9 mg/5 ml water). Right: The Tauc plot of Pd-Fe₃O₄-GO used to determine the apparent band gap energy, E_g' .

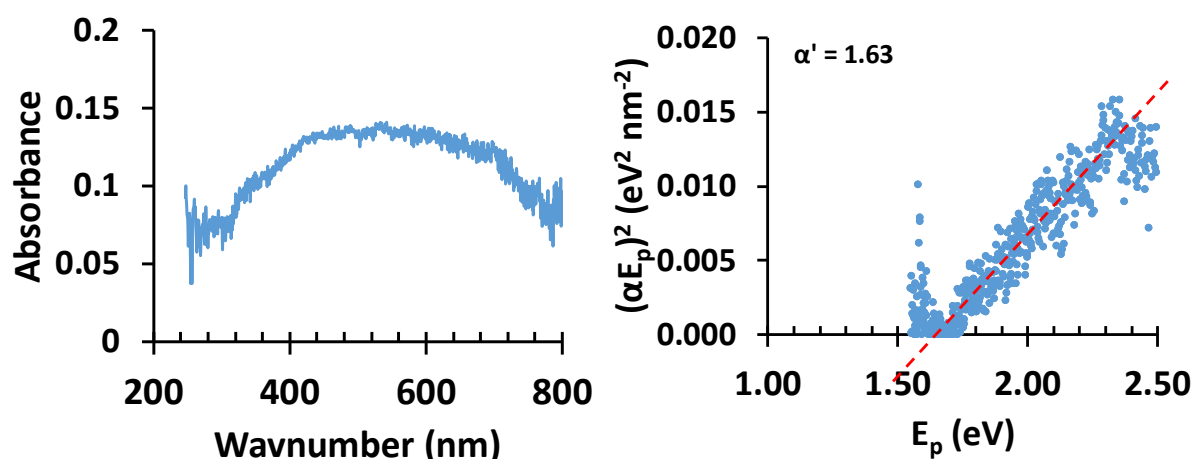


Figure S13. Left: The UV-Visible spectra of Pd-CNT-GO (3.02 mg/5 ml water). Right: The Tauc plot of Pd-CNT-GO used to determine the apparent band gap energy, E_g' .

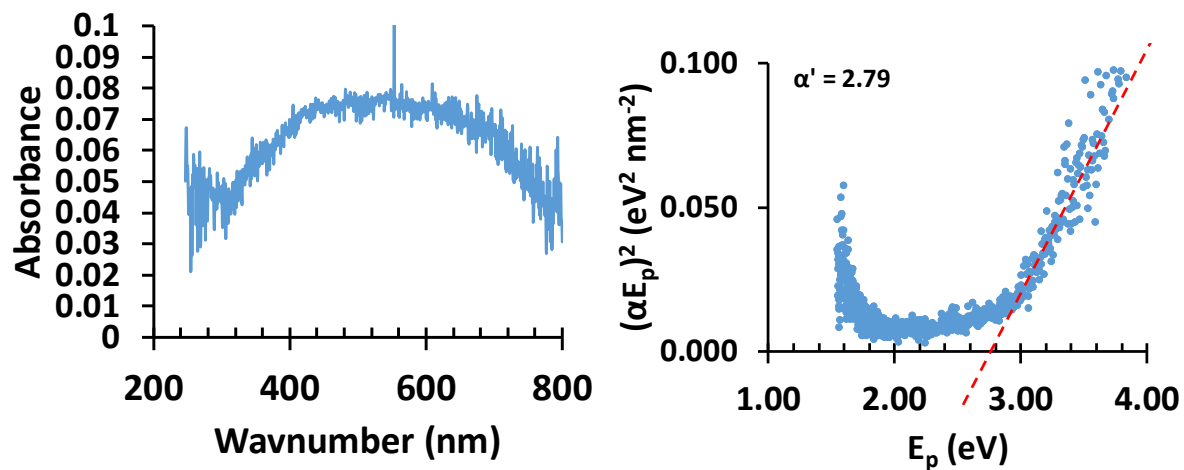


Figure S14. Left: The UV-Visible spectra of Pd-Fe₃O₄-CNT-GO (0.7 mg/5 ml water). Right: The Tauc plot of Pd-Fe₃O₄-CNT-GO used to determine the apparent band gap energy, E_g' .

Catalysis

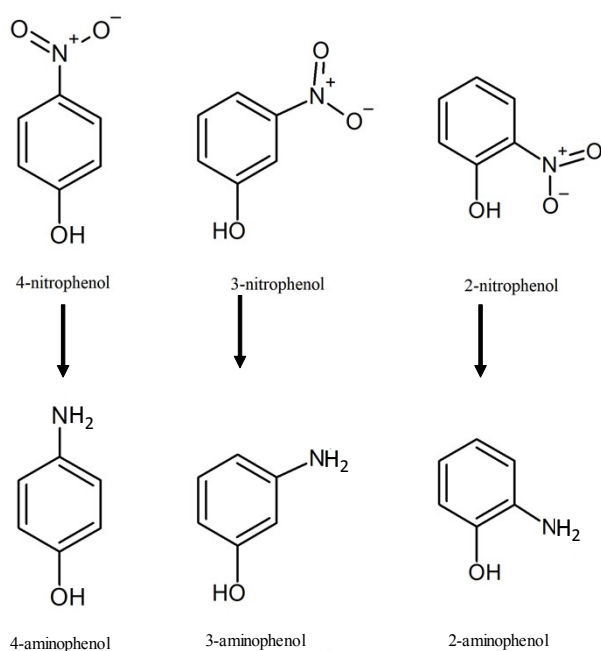


Figure S15. Structures of the reagents and products of the catalytic testing: 4-nitrophenol → 4-aminophenol, 3-nitrophenol → 3-aminophenol and 2-nitrophenol → 2-aminophenol.

UV/Vis absorption spectra of 4-NP:
Absorbance vs Wavelength (nm)

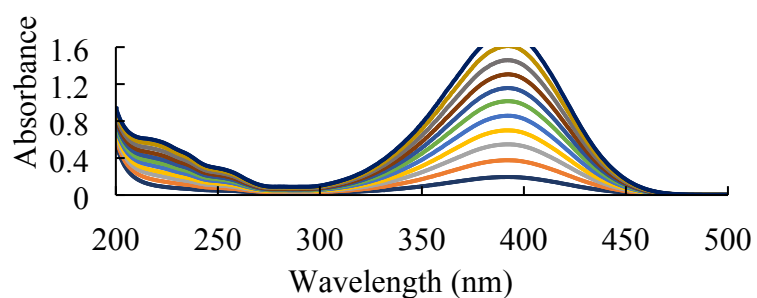


Figure S16. UV/Vis absorption spectra of 4-NP showing absorbance vs wavelength (nm) from 200-500 nm

Calibration curve for 4-NP: Absorbance vs Concentration (ppm) at 392 nm

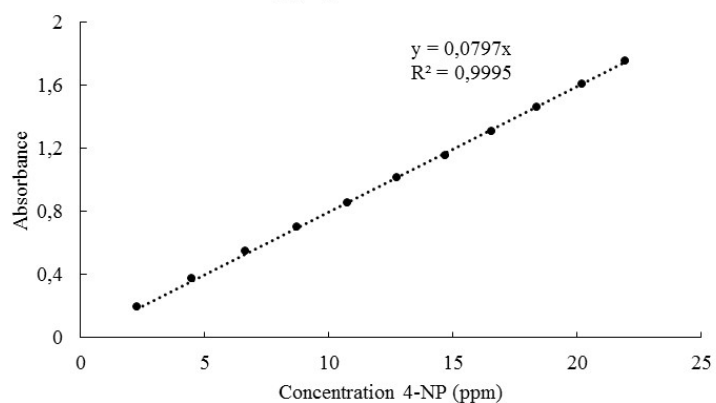


Figure S17. Calibration curve for 4-NP showing absorbance vs concentration of 4-NP (ppm) at 392 nm

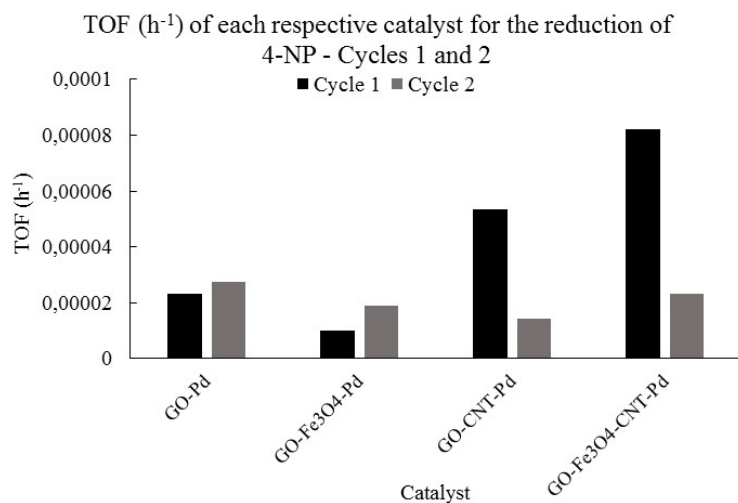


Figure S18. TOF (h^{-1}) values for each respective catalyst for cycle 1 (black) and cycle 2 (grey) for the reduction of 4-NP.

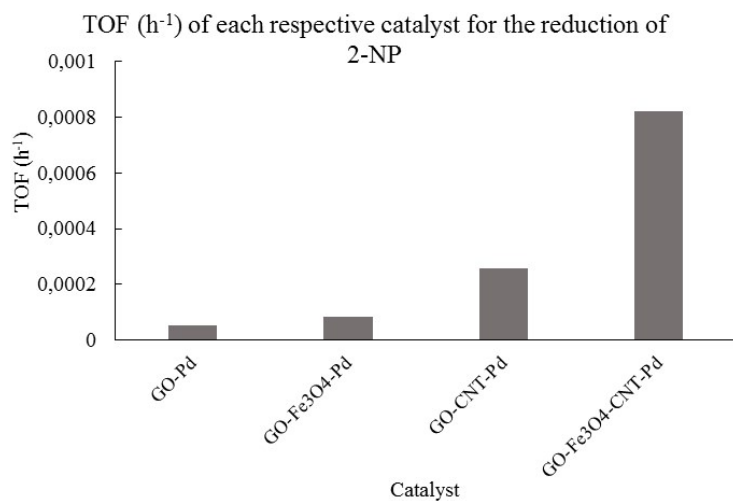


Figure S19. TOF (h^{-1}) values for each respective catalyst for the reduction of 2-NP.

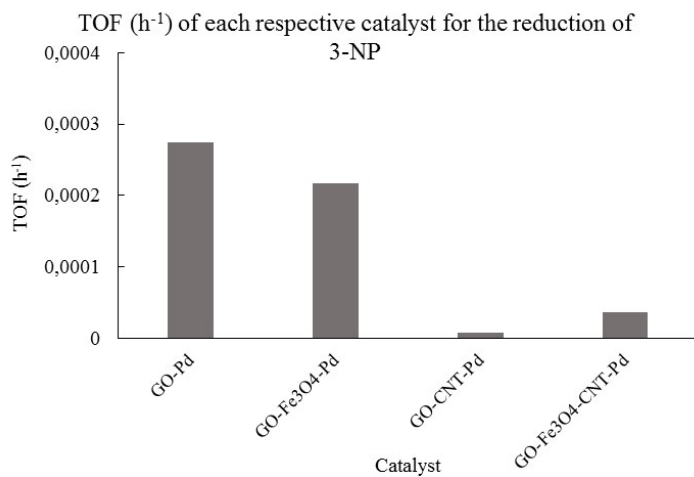


Figure S20. TOF (h⁻¹) values for each respective catalyst for the reduction of 3-NP.

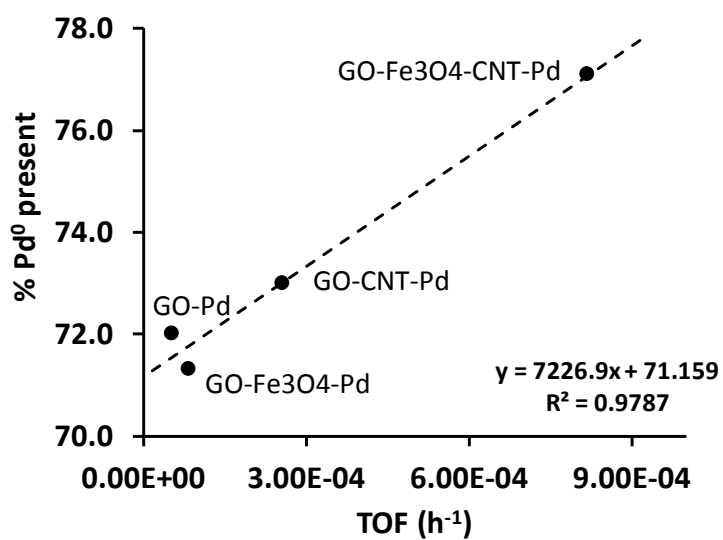


Figure S21. Relationship between the % Pd⁰ present for each composite and the TOF (h⁻¹) for 2-nitrophenol.

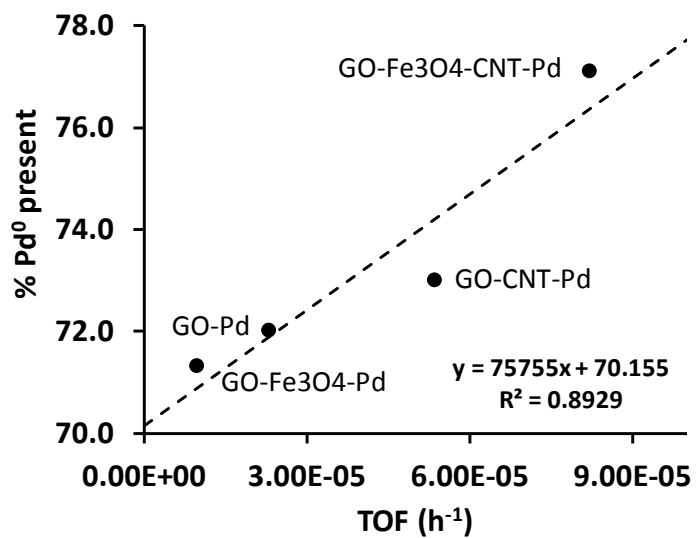


Figure S22. Relationship between the % Pd⁰ present for each composite and the TOF (h⁻¹) for 4-nitrophenol.